VOL. 23, NO. 3, 2024, 6-18
elektrika.utm.my
ISSN 0128-4428

ELEKTRIKA
Journal of Electrical Engineering

# Advanced Harmonic Mitigation in Photovoltaic Grid-Connected Systems: Jellyfish Search Optimization Approach

**Hashim Ali I. Gony**[1,2], **Ghamgeen Izat Rashed**[1,2*], **Ansumana Badjan**[1,2], **Ahmed O. M. Bahageel**[1,2] and **Husam I. Shaheen**[3]

[1]Hubei Engineering and Technology Research Center for AC/DC Intelligent Distribution Network, School of Electrical Engineering and Automation, Wuhan University.Wuhan 430072, Hubei Province, China
[2]School of Electrical Engineering and Automation, Wuhan University, Wuhan 430072, Hubei Province, China
[3]Changsha University, Changsha, Huhan, China.

[*]Corresponding author: ghamgeen@whu.edu.cn

**Abstract:** Increasing prevalence of nonlinear loads (NLL) in modern power systems poses significant challenges, particularly in terms of harmonic distortion. This distortion degrades the performance and efficiency of photovoltaic (PV) grid-connected systems (PV-GCS), demanding advanced control strategies. This study presents a unique optimization-based method that employs the Jellyfish Search Optimization (JSO) algorithm to enhance the Shunt Active Power Filter (SAPF) for effective harmonic reduction in PV-GCS with a high penetration of NLL in the distribution network. The study aims to reduce total harmonic distortion (THD) and regulate the DC-bus voltage ($V_{dc}$) in SAPF. A comprehensive comparison examination is performed between JSO and three frequently utilized optimization algorithms: genetic algorithm (GA), particle swarm optimization (PSO), and golden eagle algorithm (GE), to investigate the efficiency of JSO algorithm. The reduced THD by the JSO is only 1.32 percent, smoothly regulated the $V_{dc}$ with a short settling time, without overshooting. These findings indicate that JSO outperforms others, emphasizing that it has the potential to improve power quality (PQ) in PV-GCS with NLL. This study presents a strong foundation for minimizing harmonics in PV integrating to the grids, which contributes to improved system reliability and efficiency.

**Keywords:** PV Grid-Connected, Shunt Active Power Filter (SAPF), Harmonic Mitigation, Jellyfish search Optimization, Golden Eagle



*Article History: received 3 February 2024; accepted 2 October 2024; published 30 December 2024.*

## 1. INTRODUCTION

Renewable energy sources (RES), particularly solar PV and wind energy, are growing rapidly and being increasingly utilized. Due to their potential to overcome energy and environmental concerns [1]. There are several methods for employing solar energy, such as solar heating, solar photovoltaic thermal (PVT), solar hybrid systems and solar photovoltaic (solar PV). Lately, solar PV has become a crucial global trend and is tending to change the existing electric grid structure. Solar PV power systems face challenges due to intermittency and difficulty maintaining a continuous supply. This fluctuation may negatively influence the electric power grid. Resulting voltage variations, frequency changes, reactive power problems, and system outage [2]. Solar PV system's flexibility for grid integration promotes rapid technical progress exceeding the other RES. The adaptability of Solar PV is a key replacement for the conventional electrical network. This explains the reason behind their widespread application. Solar PV systems can be stand alone or grid connected. PV-GCS are superior to stand-alone PV systems. Since battery storage systems are not required [3].

The redundancy of NLL applications in modern electric grids threatens grid stability, particularly when solar is integrated to the grid [4]. The argument reveals security risks such as harmonics, reactive power difficulties, and voltage fluctuation. Harmonics generated by NLL reduce system efficiency by producing losses. Harmonics can cause transformer overheating, communication signal interference, and disturb machinery's functioning. Harmonic could impact the entire grid from end-to-end, including consumers [5].

Traditionally, PQ issues have been solved through passive filters. Passive filters have some drawbacks, most notably that they are bulky and fixed, making adjustment problematic [6]. Recently, customer devices or (flexible AC transmission systems) FACTS have been provided as alternatives, like (static synchronous compensator) STATCOM, (dynamic voltage regulator) DVR, and SAPF [7]. Among FACTS devices, SAPFs stand out for their better flexibility and capability to capture and mitigate PQ issues. These advantages make them more convenient than

passive filters. SAPFs have proven highly effective for PV-GCS and meeting grid requirements by maintaining reliability in the presence of NLL within the power system. These devices require accurate design for their parameters and an effective control strategy for efficient operation. Researchers have developed various techniques and methods for controlling SAPF in the context of PV systems. [8].

SAPFs act as current controllers, injecting compensatory currents. These currents, which are identical in magnitude but opposite in phase and block undesired harmonic signals. Basically, SAPFs are (voltage source inverters) VSI consist of six (IGBTs, MOSFETs or GTOs) switches. The control technique depends on the tuning procedure of these VSI switches [9] To achieve their objectives, SAPFs are typically connected in parallel with the harmonic source at the point of common coupling (PCC). SAPFs stand out for their adaptability and high satisfaction with compensation capabilities, effectively keeping THD within the IEEE-519 standard. Their control methods comprise classical methods and intelligence-based methods, which smoothly integrate PQ challenges [10].

Advanced researches focused on enhancing control approaches employing artificially intelligent tactics and optimization algorithms. The outcomes indicate potential improvement in system performance and contribute to successfully reducing THD within standard; nevertheless, harmonic events have been the subject of comprehensive researches in recent decades, particularly in PV-GCS [11].

Harmonic mitigation using algorithms implies the use of optimization and control approaches to reduce THD in power systems. Several studies have investigated applying different algorithms for this objective, including metaheuristic optimization and predictive algorithms. These algorithms are developed to assess, detect, and mitigate harmonic components in power systems, eventually enhancing PQ. Specific algorithms used for harmonic mitigation include evaluation-based algorithms (e.g., GA), swarm-based algorithms (e.g., PSO, anti-lion optimizer), and predictive algorithms for generating reference current in an active power filter. Metaheuristic algorithms are critical for harmonic elimination due to their efficient response to the complicated optimization problem [12]. This highlights their importance in addressing the harmonic distortion issue. As a result of their adoption in power systems, this research reveals ongoing efforts to find effective algorithmic solutions for minimizing harmonics in power systems.

The work in [13] proposed a proportional-resonant controller improved by GA for SAPF control. The method reduces THD from 20.2 to 4.2 for R-L loads and 56.1 to 4.5 for R-C loads, with a unity power factor, demonstrating its effectiveness. The paper presents a 7-level multi-level (MLI) inverter designed for PV applications, utilizing a hybrid Harris-Hawks optimization with PSO (HO-PSO) algorithm to optimize switching angles of active filter. The hybrid algorithm, as implemented, shows improved performance with low harmonic distortion of 2.82% and minimal switching losses [14]. The study in this paper introduces a redesigned H-Bridge MLI construction with increased voltage levels, reduced switching losses, and fewer components. It uses asymmetrical input voltage sources and the JAYA algorithm to reduce harmonic distortion, achieve quick acceleration, and reduce computational overhead [15]. This study explores proportional-resonant regulators in SAPF to manage grid currents and reduce harmonic distortion. Three adaptive algorithms are developed to maximize dc-link voltage and improve grid current quality by compensating for severe harmonics. Experimental findings confirm their practicality [16]. This work aims to improve constant instantaneous power management by applying a new adaptive Autarchoglossans lizard foraging algorithm (AALF) algorithm to a three-phase active power filter with a solar PV array on its DC-bus [17]. These algorithms meet several challenges, like Complexity and parameters such as low convergence and sensitivity to parameter settings are major drawbacks for these algorithms, limiting their ability to extensively explore the solution space, impacting their exploration capabilities, and perhaps leading to poor solutions if not well handled [18].

The JSO algorithm is a powerful and robust optimization tool, displaying great efficiency in modern research indicators. The JSO algorithm is designed to deal with the complications of generating maximum power from PV systems, and this becomes more difficult with fluctuations in solar irradiation, temperature, and load variation [19]. Employing the JSO algorithm for maximum power point tracking (MPPT), researchers are willing to improve the performance of PV-GCS, adding to the global effort to satisfy growing energy demand while solving the global energy crisis [20]. To verify the advantages of the JSO algorithm over existing algorithms, it has been confirmed and implemented using Matlab/Simulink as well as physical experiments. The suggested algorithm has shown favourable findings in many circumstances, including partially shading situations for solar PV systems, emphasizing its ability for practical applications in enhancing the efficiency of PV systems. As a result of JSO's success in overcoming PV system challenges, it is described as an innovative strategy that has possibilities for boosting efficiency [21].

This paper identifies a research gap on: (i) the limited exploration of the JSO algorithm to optimize SAPF in PV-GCS; (ii) the existing literature lacks of detailed analysis of dual objectives for THD control and $V_{dc}$ voltage regulation of SAPF in PV-GCS under NLL. (iii) Furthermore, the literature highlights the need for comparative analysis of the JSO algorithm with other algorithms in the aspect of THD reduction and $V_{dc}$ regulation in PV-GCS. This study fills a well-defined gap by utilizing the JSO algorithm to reduce harmonics in PV-GCS under NLL. To demonstrate the efficiency of JSO, a comprehensive comparative analysis is proposed for both THD reduction and enhancement of $V_{dc}$ voltage. This analysis employs a well-known optimization technique, including GA, PSO, and GE algorithms. The study aims to investigate the JSO's superiority in harmonic suppression and $V_{dc}$ voltage regulation. The following part explains the system modelling. The system modeling and design are given and analyzed in Section 2. Finally, Section 3

illustrate the discussion of the obtained results followed by conclusion.

## 2. SYSTEM MODELING AND DESIGN

The proposed model, shown in Figure. 1, illustrates the general structure of a PV-GCS coupled with a SAPF. The PV panels are connected to a low voltage (LV) grid, which provides electricity to a variety of loads. The system operates on a real low-voltage feeder in Sudan's power distribution network. The primary objective of this design is to reduce harmonic distortions and provide a high-quality power supply. The SAPF plays a key role in this process by injecting compensating current. To ensure optimal SAPF performance, optimization algorithms have been utilized such as the JSO algorithm. These methods are employed to fine-tune the (proportional-integral) PI controller parameters ( $k_p, k_i$ ) in the SAPF, ensuring effective harmonic mitigation and increase power system stability.

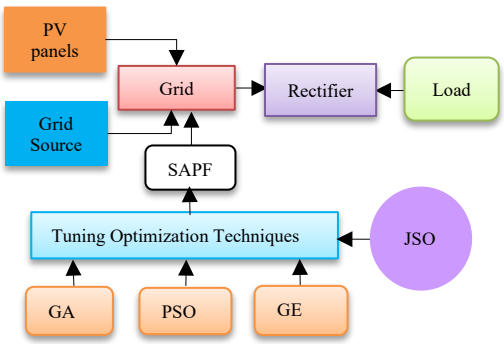


Figure 1. Basic Diagram of PV-GCS

### 2.1 Grid Side

The load configuration utilized in the LV feeder contains diode rectifier loads. These loads are known for their characteristics of withdrawing non-sinusoidal currents, leading to grid current distortion, which creates complexity due to their nonlinear features. The nonlinear behavior is generally produced by converting parts that cause current surges during switching events, resulting in harmonic distortions and lower system performance. While a PV system is connected to the grid, the conversion stages, such as DC boost converters and inverters, complicate matters even further. These issues demand precise analysis and design considerations in order to achieve the best performance and reliability. Control strategies are critical for minimizing the harmful impacts of harmonics, improving grid stability, and increasing system efficiency.

### 2.2 Solar PV System

The proposed model 1 MW solar PV station is linked to the LV grid via a three-phase inverter. The inverter is set up to perform at a unity power factor to inject only active power into the grid. In the context of inverter control, the PQ theory is applied to generate the required PWM signal for switching IGBTs of VSI. The DC boost converter is configured to receive the PV output and step-up it to a limited value, employing the Perturb and Observe (P&O) algorithm for MPPT. The power output of the PV generator, denoted as $P_{PV}$, can be approximated in sets with low mean temperatures by applying the following equation: [22].

$$P_{PV} = P_{PV,rated} * \frac{G}{G_{ref}}\left[1 + \beta_{ref}\left(T_C + T_{ref}\right)\right] \quad (1)$$

In the above equation, $P_{PV,rated}$ represents the PV module's rated power output in kW, and G represents the hourly global irradiation on the module surface in kW/m$^2$. G represents the standard incident radiation of 1 kW/m$^2$, whereas $T_{ref}$ represents the temperature coefficient. $T_C$ denotes the solar cell temperature, which can be calculated using equation (2):

$$T_C = T_a + \frac{T_{NOCT} - 20}{800} * G \quad (2)$$

Where, $T_a$ is the ambient temperature in degrees Celsius (C$^\circ$), while $T_{NOCT}$ is the cell temperature of a PV module operating at 25 C$^\circ$ and 1 kW/m$^2$ of solar radiation. The dynamics of the PV generator can be described as:

$$V_{PV} = R_{PV} I_{PV} + L_{PV} \frac{dI_{PV}}{dt} + V_{dc} \quad (3)$$

The PV array's voltage and current are denoted as $V_{PV}$, and $I_{PV}$ respectively. The resistance and inductance of the DC wire are $R_{PV}$ and $L_{PV}$, respectively. *The SunPower* SPR-445NX-WHT-D module was used in this analysis. The PV system is designed to generate ~1MW at 1kw/m$^2$ irradiance and includes 375 parallel strings with 6 series modules per string. Figure 2 depicts the PV solar I-V and P-V characteristics under various irradiation levels. The PV output voltage at the maximum power point is 460V.

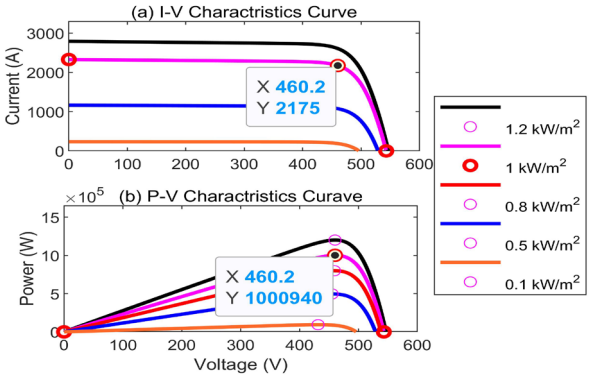


Figure 2. I-V and PV Characteristic of PV

In a real-world power system, variations in solar irradiance and temperature directly impact the output of PV modules. To assure the optimal performance of PV solar systems, Figure 3 and 4 illustrate the irradiance and temperature fluctuations, respectively, during a day. While variations in solar irradiance and temperature have a direct impact on PV module production. The variation in sun irradiation has a considerable impact on the output of PV solar systems. Solar irradiation, or the power per unit area received from

the sun, is an important component in determining the electrical energy provided by PV panels.

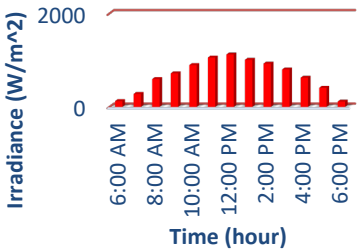


Figure 3. Hourly Irradiance Variation

Temperature affects both the voltage and the efficiency of PV. Typically, an increase in temperature reduces the open-circuit voltage of PV, limiting the overall power output. However, the current slightly increases with temperature, but this effect is frequently less important than the voltage drop.

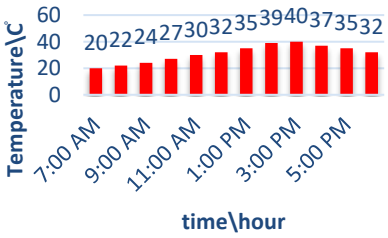


Figure 4. Hourly Irradiance Variation

The MPPT continuously assesses variations in PV output voltage due to irradiance and temperature change. This tracking makes real-time modifications to maximize PV energy production and efficiency.

### 2.3 Shunt Active Power Filter

The VSI is the backbone of the SAPF. It composed of two circuits: the control circuit and the power circuit. The control circuit consists of a DC-bus capacitor ($C_{dc}$) with its terminal $V_{dc}$ voltage as shown in Figure 4, and the main objective is to extract the required current signal for compensation. The control circuit's purpose is to detect any change in the harmonic signal and identify instant reference compensation. The power circuit is designed to generate the necessary pulse width modulation (PWM) signal and work in synchronization to maintain a constant terminal voltage level by storing energy in the capacity. The fundamental objective of the control circuit is to consistently monitor and track any alterations or deviations in the current harmonic signal and generate the reference compensating signal. SAPF accuracy is predominantly influenced by the applied reference current extraction technique. Prior to SAPF installation, the current flow in the grid can be expressed in an equation (4).

$$i_S = i_L = i_{1L} + i_H \tag{4}$$

Here, $i_S$, $i_L$, $i_{1L}$ and $i_H$ are refer to the source current, load current, fundamental form of the load current, and harmonic form current, respectively.

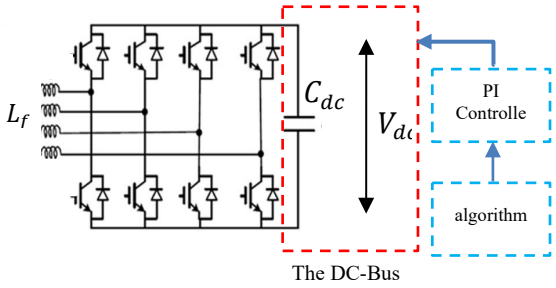


Figure 5. VSI and DC-Link Components of SAPF

After SAPF is inserted at PCC, extra two currents appear, the required harmonic compensation signal generated by the SAPF, having the same magnitude as the harmonic current with 180◦ phase shift, and the $V_{dc}$ voltage necessary to maintain the capacitor terminal voltage at the required discharge level. Consequently, the current flow in the grid can be estimated as refer to the source current, load current, fundamental form of the load current and harmonic form current, respectively. Consequently, current flow in grid can be estimated as:

$$i_S = i_L = [i_{1L} + i_H] - i_C + i_{dc} \tag{5}$$

$$i_S = i_{1L} + i_{dc} \tag{6}$$

Where, $i_C$ refers to the injected current for compensation, and $i_{dc}$ stands for the DC-bus current. To generate a typical harmonic compensating signal that reflects the harmonic current signal, it is crucial to maintain the limited designed value and evaluate it under accurate assumptions because the terminal voltage of the capacitor is the only factor responsible for determining the required harmonic compensating current signal. In this scenario, they counteract each other, as in equation (5), causing the grid's current to assume a sinusoidal shape in relation to the basic frequency [23].

#### *2.3.1 P-Q Theory for SAPF Control*

The extraction of harmonic signals is a very crucial process that significantly influences the effectiveness of the SAPF to mitigate harmonic and system performance, and the overall accuracy of the SAPF depends on it. Various techniques have been developed for extracting harmonic signals to evaluate the reference current, broadly classified as time domain approaches techniques and frequency domain approaches techniques [24].

$$\begin{bmatrix} v_0 \\ v_\alpha \\ v_\beta \end{bmatrix} = \sqrt{\frac{2}{3}} \cdot \begin{bmatrix} 1/\sqrt{2} & 1/\sqrt{2} & 1/\sqrt{2} \\ 1 & -1/2 & -1/2 \\ 0 & \sqrt{3}/2 & \sqrt{3}/2 \end{bmatrix} \cdot \begin{bmatrix} v_a \\ v_b \\ v_c \end{bmatrix} \tag{7}$$

$$\begin{bmatrix} i_0 \\ i_\alpha \\ i_\beta \end{bmatrix} = \sqrt{\frac{2}{3}} \cdot \begin{bmatrix} 1/\sqrt{2} & 1/\sqrt{2} & 1/\sqrt{2} \\ 1 & -1/2 & -1/2 \\ 0 & \sqrt{3}/2 & \sqrt{3}/2 \end{bmatrix} \cdot \begin{bmatrix} i_a \\ i_b \\ i_c \end{bmatrix} \quad (8)$$

Time domain techniques are dependent on algebraic transformations and circuit analysis, they require fewer calculations, on the other hand, frequency domain approaches are more complicated and necessitate advanced processing memory. The time domain instantaneous reactive power or (P-Q) theory is employed for this study. The source voltage and current are transferred form rotating form into stationary form [25]. Where $v_a$ , $v_b$ , $v_c$ , and $i_a$ , $i_b$ , $i_c$ are the rotating coordinate forms of the three-phase grid voltages and currents; correspondingly, and represent the three-phase voltages and currents in the stationary zero-α-β forms, respectively, to eliminate zero sequences in the α-β coordination, according to the following equations to evaluate the complex sum of the reactive power (Q) and active power (P) as:

$$S = P + jQ = v_{\alpha\beta} i^*_{\alpha\beta} = (v_\alpha - jv_\beta)(i_\alpha + ji_\beta) \quad (9)$$

$$Or\ S = (v_\alpha i_\alpha + v_\beta i_\beta) + j(v_\alpha i_\beta - v_\beta i_\alpha) \quad (10)$$

$$\begin{bmatrix} P \\ Q \end{bmatrix} = \begin{bmatrix} v_\alpha & v_\beta \\ -v_\beta & v_\alpha \end{bmatrix} \cdot \begin{bmatrix} i_\alpha \\ i_\beta \end{bmatrix} \quad (11)$$

Here, S, P, Q, and * denote the complex power, active power, reactive power, and complex conjugate, respectively. Simultaneously, the instantaneous active and reactive power components (P and Q) can be calculated from equations (9) and (10), (11). In the presence of harmonic source in the grid, the instantaneous P and Q components are analyzed into their AC and DC origin forms, as shown in equations (12) and (13). Figure 6 illustrates the DC components ($p^-$) of the instantaneous P correspond to the fundamental voltage waveform and current values. These DC forms represent the power transferred from the grid to the load; hence the AC components ($p^\sim$) signify the energy circulating between the grid source and the load [26].

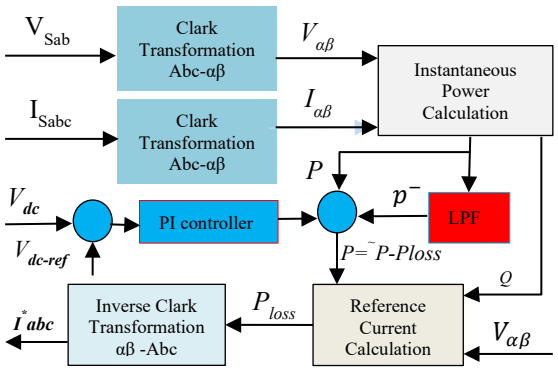


Figure 6. P-Q Theory Diagram

The three-phase AC source should only supply instantaneous real power, including PV solar, which is generated through a high-order low-pass filter as presented in Figure 6. These $p^-$ and $q^\sim$ are the fundamental components, harmonic components of the instantaneous Q components due to energy circulation between the load and grid source as:

$$P = p^- + p^\sim \quad (12)$$

$$Q = q^- + q^\sim \quad (13)$$

$$P^\sim = P - p^- + p^-_{loss} \quad (14)$$

$$\begin{bmatrix} i^*_\alpha \\ i^*_\beta \end{bmatrix} = \frac{1}{v^2_\alpha + v^2_\beta} \cdot \begin{bmatrix} v_\alpha & v_\beta \\ v_\beta & v_\alpha \end{bmatrix} \cdot \begin{bmatrix} P^\sim \\ Q \end{bmatrix} \quad (15)$$

Either the total P or Q of AC components is critical in estimation because the SAPF dissipates a tiny amount of actual Q from the AC source and external power supply.

$$\begin{bmatrix} i^*_a \\ i^b_* \\ i^*_c \end{bmatrix} = \sqrt{\frac{2}{3}} \cdot \begin{bmatrix} 1 & 0 \\ -\frac{1}{2} & \frac{\sqrt{3}}{2} \\ -\frac{1}{2} & -\frac{\sqrt{3}}{2} \end{bmatrix} \cdot \begin{bmatrix} i^*_\alpha \\ i^*_\beta \end{bmatrix} \quad (16)$$

In order to compensate for the VSI losses while keeping the AC form of the active power, the total Q is required. To compensate for the VSI switching losses and to keep the voltage within the desired boundary, the total Q is calculated from equation (15), and the compensation reference currents in the α-β forms are measured by equation (16), which is then transformed through the inverse transformation to the a-b-c form.

### *2.3.2 Current Control Technique*

To implement SAPF's current control, various control techniques have been used to generate the control pulses which are necessary in determining the operation of the filter switching status. During this study, the hysteresis current band (HBC) in Figure 7 is proposed in order to extract the switching PWM signals of the VSI, HBC control technique has large scale application because it is simple in configuration, fast in response, high accuracy and reliable.

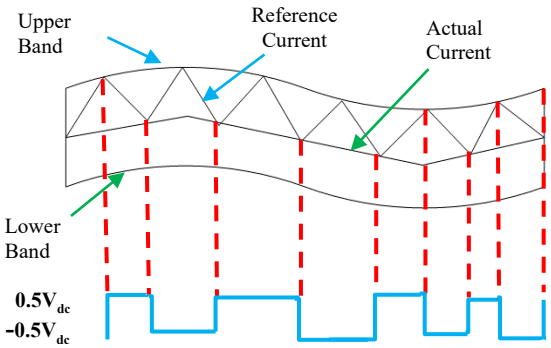


Figure 7. Hysteresis Band Current Control Logic

The HBC is a simple technique for PWM switching signal generation with comparatively good current loop response, the actual phase current is compared to the sinusoidal wave reference current which is produced by the control circuit. In HBC control, the current is maintained in a reference predefined band of width, as shown in Figure 7. The three-phase source current ( $i_{Sa}, i_{Sb}$ *and* $i_{Sc}$ ) is calibrated to the reference current $i_{Sa}^*, i_{Sb}^*$, *and* $i_{Sb}^*$ and the VSI gates continuously are on and off in accordance with the error to keep the actual current within the band.

The DC bus elements $V_{dc}$ and $C_{dc}$ can be estimated by the following equation.

$$C_{dc} = \frac{2P_{Load}}{V_{dc}^2 - V_{dc,min}^2} \tag{17}$$

$$V_{dc} = \sqrt{2}.V_m \sqrt{\frac{P_{Load}(1+\eta)}{C_{dc} f_{sw}}} \tag{18}$$

Where; $P_{Load}$ is the maximum power send to the grid. And $V_{dc}$ is the capacitor terminal voltage estimated, $V_{dc,min}$ is the minimum terminal voltage, $V_m$ is the peak value of AC voltage, $\eta$ is the power losses in the filter, and $f_{sw}$ is the switching frequency of the VSI. A PI controller is utilized in the voltage control loop to maintain constant $V_{dc}$ voltage and compensate for harmonic current. The difference between the capacitor terminal voltage and reference DC voltage is applied to the PI controller, eliminating steady-state error ( $V_{dc} - V_{dc\,ref}$ ) in monitoring reference current. The gain $G_i(s)$ indicate the transfer functions of the PI controller and VSI of the SAPF. When the six switches of the VSI are operated at a high frequency, the amplitudes of ($i_{Sa}, i_{Sb}$, *and* $i_{Sc}$) are nearly equivalent to the magnitudes of ($i_{Sa}^*, i_{Sb}^*$, *and* $i_{Sc}^*$). Assume the closed-loop current controller transfer function is unity

$$G_i(s) = \frac{i_{Sabc}}{i_{Sabc}^*} = 1 \tag{19}$$

Where $i_{Sa}$, $i_{Sb}$ , and $i_{Sc}$ indicates the three-phase source current, and $i_a^*, i_b^*, i_c^*$ correspond to the three-phase reference current. The parameters of PI controller's $k_p$ gain and $k_i$ gain, can be estimated via the step response of the closed loop block diagram in Figure 8. As a result, the transfer function of the PI closed loop of the $V_{dc}$ is obtained from the equation (20):

$$\frac{v_{dc}}{v_{dc-ref}} = \frac{\frac{k_p.k_i}{C}}{s^2 + \frac{k_p}{C}.S + \frac{k_p.k_i}{C}} \tag{20}$$

The equation (20) includes $V_{dc}$ is the DC-bus voltage, $V_{dc-ref}$ is the DC-bus reference voltage, $k_p$ is the proportional gain, $k_i$ is the integral gain, and C is the DC-bus capacitor.

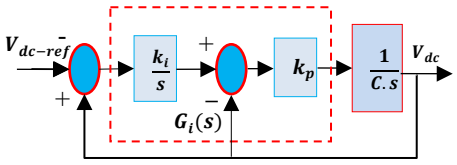


Figure 8. PI Controller and Error Signal Estimation

The $V_{dc}$ closed loop control model in above Figure 8 demonstrates a transfer function similar to a second-order system. Accurately estimating $k_p$ and $k_i$, this technique ensures the control system's response aligns with a typical second-order system, improving system performance and stability under fluctuating conditions.

$$H(s) = \frac{w_n^2}{s^2 + 2\zeta w_n s + w_n^2} \tag{21}$$

Where; ζ denotes the damping factor, $w_n$ is the natural frequency damping. By combing Equation (22) Equation (23)

$$\frac{k_p}{C} = 2\zeta \mathrm{w}_n \;\; and \;\; \frac{k_p.k_i}{C} = w_n^2$$

Hence, $k_p = 2\zeta \mathrm{w}_n C \; and \; k_i = \frac{w_n}{2\zeta}$

$$I_s(t) = I_L(t) - I_f(t) \tag{22}$$

$$V_s(t) = V_m sin\omega t \tag{23}$$

### 2.4 SAPF Tuning Optimization

Frequently, meta-heuristic optimization algorithms have been widespread and become popular for addressing diverse complex challenges because (i) their ideas are simple and easier to construct; (ii) information about the objective function gradient is not required; (iii) they can navigate around local minima; and (iv) they are applicable for evaluating and solving a broad range of problems across various fields. Advanced processing computers are needed due to their application of metaheuristics, which depends on enhancing and expediting the execution of these algorithms [27]. Leveraging metaheuristic approaches such as GA, PSO, GE, and JSO can significantly increase SAPF performance by optimizing PI controller parameters.

The GA is an ecological optimization technique based on natural selection and genetics. GA, established by John Holland in the 1970s, uses mechanisms such as selection, crossover, and variation to generate a population of potential answers across generations. In the framework of SAPF, GA's ability to investigate a substantial search space makes it powerful for identifying optimal parameter settings. However, early convergence, computation complexity, and a high sensitivity to parameter change can all limit GA's performance in dynamic and complicated power systems [28]. PSO was developed by Kennedy and Eberhart in 1995 and reaches optimal solutions by

imitating the social behavior of birds moving or fish schooling. Each particle in the swarm indicates a potential solution while it moves through the search space, effected by its own and neighboring particles. PSO is known for its ease and high convergence, making it ideal for SAPF optimization. Nonetheless, PSO may encounter a slowdown where particles rapidly converge to local optima, and its efficiency is basically dependent on the parameter variables of the system [29]. The GE is a relatively recent metaheuristic inspired by the hunting tactics of golden eagles. Its objective is to balance both discovery and extraction by modeling the dynamic behavior of eagle hunting. GE has proven itself in different optimization processes due to its flexibility and effectiveness in maintaining a balance between global and local searches. For SAPF tuning, GE's balanced examination can produce robust solutions. However, it requires careful parameter tuning, particularly with dynamic systems, which can be challenging and computationally intensive [30].

### 2.5 Artificial Jellyfish Search Optimization (JSO)

The JSO is an advanced optimization technique inspired by jellyfish's natural motion in ocean currents. This algorithm simulates two types of motion: passive movements influenced by ocean currents and active movements aimed at finding food. By using these behaviors, JSO efficiently explores and exploits the search space to discover the best solution. Its unique balance of passive and active motions, allows it to efficiently optimize control parameters, resulting in considerable gains in harmonic mitigation and overall power quality [31]. The proposed JSO algorithm relies on three principles, as shown in Figure 9. Initially, jellyfish exhibit movement either towards the ocean current or within the swarm, with a "time control mechanism" regulating the transition between these movements. Secondly, they navigate through the ocean, seeking food in areas abundant with resources. Thirdly, the quantity of food discovered is evaluated based on the location and its associated objective function. As shown in Figure 9, the direction of the ocean current ($trend^{\rightarrow}$) is determined by summing the average of all vectors from each jellyfish in the ocean to a jellyfish located in the best position, as in equations (24, 25).

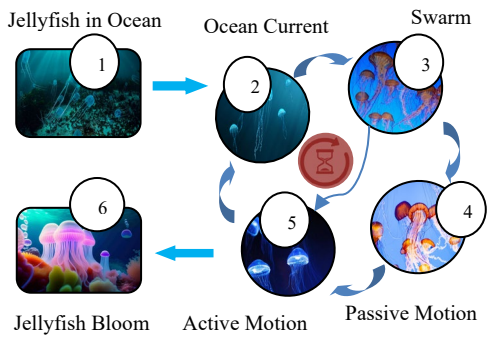


Figure 9. Jellyfish and Ocean Current

Each jellyfish can adjust its position using the equation (26), where $n_{Pop}$, $X^*$, $e_c$ and $\mu$ represent the number of jellyfish, the current location of the best jellyfish in the swarm, the attraction factor, and the mean location of all jellyfish, respectively. β is the distribution coefficient typically > 0. Jellyfish exhibit either passive motion (Type A), characterized by motion around their location, especially during swarm formation, or active motion (Type B), which tends to dominate over time. The updated location of each jellyfish is determined by equation (27), where $U_b$, $L_b$ denote the lower bound, upper bound of each space, and γ the swarm motion coefficient, respectively.

$$trend^{\rightarrow} = \frac{1}{n_{Pop}} \sum trend^{\rightarrow}{}_i = \frac{1}{n_{Pop}} \sum (X^* - e_c X_i) \quad (24)$$

$$\text{Or} \quad trend^{\rightarrow} = X^* - e_c \frac{\sum X_i}{n_{Pop}} = X^* - e_c \mu \quad (25)$$

$$X_i(t+1) = X_t(t) + rand(0,1)(X^* - \beta) rand(0,1)\mu \quad (26)$$

$$X_I(t+1) = X_i(t) + \gamma . rand(0,1).(U_b - L_b) \quad (27)$$

A time control mechanism is employed to regulate jellyfish movement in equation (28), determining whether they follow the ocean current or move within the jellyfish swarm. Here, hence c(t), t and $Max_{iter}$ refer to the control time function, iteration number time, and the maximum iteration, respectively [32].

$$c(t) = \left| \left(1 - \frac{1}{Max_{iter}}\right) . 2. (2. rand(0.1) - 1) \right| \quad (28)$$

## 3. RESULTS AND DISCUSSION

The simulation model in Figure 10 illustrates the Simulink model of the utility grid without a PV system, which consists of a three-phase AC voltage supply and multiple loads. The solar PV system has a 1 MW rating and involves 375 parallel strings with 6 series modules per string. The boost converter receives the PV output voltage, then steps up to a setting level. The boost converter sends output power to a three-phase inverter. The output of the inverter is directly connected to a three-phase LV feeder. P&O approach is employed to achieve the greatest power output from PV panels under varying irradiance and temperature settings. The simulation model comprises the key design components listed in Table 1. The inverter runs at a switching frequency of 10 kHz, utilizing P-Q theory for inverter control, maintaining a unity power factor to inject only active power to the grid.

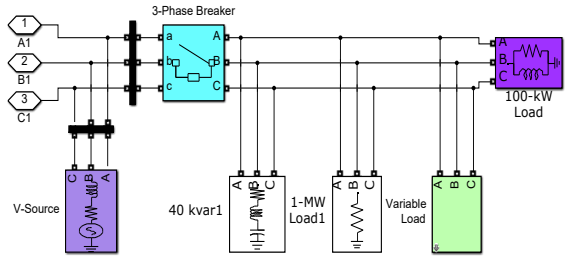


Figure 10. The Utility Grid

According to (Sudanese Electricity Distribution Company) SEDC's load data statistics, the distribution grid is facing a significant number of electronic device-based loads in the feeder, particularly during peak loads, which causes harmonic issues in the grid current, transformer overheating, and outages. Residential users do not meet the required criteria for distributing power. To precisely remove harmonic pollution induced by loads and solar PV intermittency behavior, the study will explore and mitigate THD during peak demand under a variety of irradiance conditions. This load configuration in this LV feeder is highly propagated of NLL, like VFDs and many other diode rectifier loads. The load features increase complexity due to their nonlinearity. However, the converting elements exhibit nonlinear behavior, leading to current surges during switching events that can induce harmonic distortions and reduce system performance.

Table 1. Important Model Parameters

| Parameters | Values | Parameters | Values |
|---|---|---|---|
| Grid | 450V/50Hz | SAPF $C_{dc}$ | ~220µF |
| PV Rating | 1MW | SAPF $V_{dc}$ | 800V |
| $L_{inv}$ | 644.6mH | Filter $L_f$ | 23.58mH |
| Converter $C_{dc}$ & $V_{dc}$ | 680µF & 800V | Inverter switching | 10 kHz |

Furthermore, the conversion stages, notably in PV systems, such as DC boost converters and inverters, add complexity to the grid when the PV system is connected. These events require proper analysis and design considerations to ensure the system's optimal performance and dependability. Control methods can be employed to mitigate the negative effects of nonlinearity in the grid.

### 3.1 Grid Performance Before PV System

Creating reliable and effective electrical systems in an assortment of applications demands a better understanding and regulation of system behavior. The study assessed the effectiveness of the LV network's performance by imitating the load's dynamic characteristics prior to the PV system.

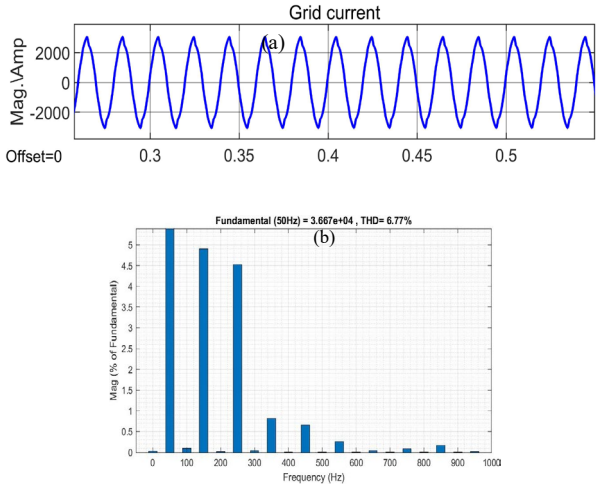


Figure 11. (a) Grid Current (b) Grid Current THD

Variable loads have been introduced to simulate the dynamic fluctuation of the loads in a real power system. The graph in Figure 11 (a) shows the grid current, and Figure 11 (b) shows grid current THD of 6.77. This distortion highlights the profound influence of the load element on the PQ, emphasizing the critical challenges of electrical grids. The growth of such deformation not only compromises the integrity of the power grid but also assures the rise of negative effects, including increased equipment heating and decreased operational reliability. This has great impact on PV integration.

### 3.2 Grid Performance with PV System

The integration of PV solar systems into the LV grid brings a number of challenges due to the corresponding energy conversion elements. Additionally, the fluctuation caused by irradiance and temperature variations increases the complexity of integration, which may have a direct impact on the grid.

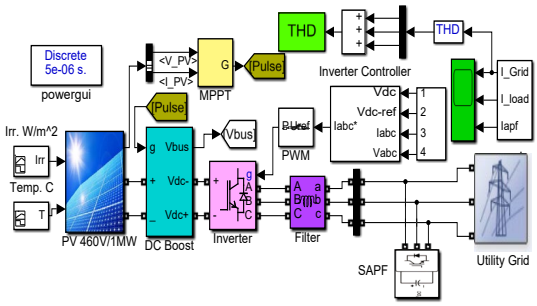


Figure 12. Simulation Mode of PV-GCS

The MPPT attempts to maintain a constant PV output voltage; however, the output current and power vary proportionally with PV input. It is crucial to consider their response to changes. The model in Figure 12 adequately simulates the entire grid with the solar PV systems by incorporating temperature and irradiance fluctuations on a daily basis. This strategy reflects the real-world situations that PV systems face. Modelling these variations improves

the understanding and prediction of PV system performance.

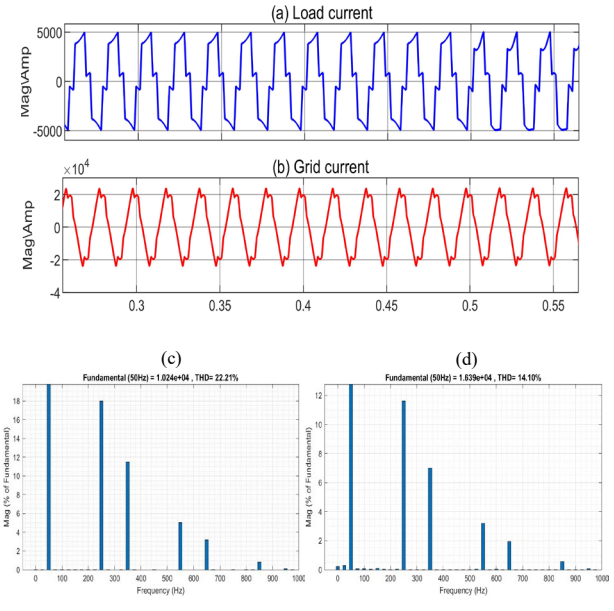


Figure 13. (a) Load Current (b) Grid Current (c) Loads Current THD (d) Grid Current THD

This modification will simulate the true nature of PV characteristics in a real word power system. Creating reliable and effective electrical systems, a better understanding and regulation of system behavior. The load current is reported in Figure 13 (a), and the load current THD is 22.21, as shown in Figure 13 (c). The grid current signal also deformed, as shown in Figure 13 (b), with a recorded THD of 14.10 as in Figure 13 (d). The distortion in grid current reflects the difficulty of integrating solar PV into such electrical network. The simulation results are a useful diagnostic tool for finding the primary contributing element to harmonic issues in the system, which is the nonlinear nature. Understanding these problems is critical for creating effective mitigation strategies that reduce harmonic distortions while improving PQ. These simulation results show crucial insights in planning and implementing mitigation techniques adapted to the individual characteristics of the PV-GCS by quantifying the degree of harmonic distortion.

### 3.3 SAPF for Harmonic Mitigation

The SAPF is strategically placed at the PCC to inject compensatory currents into the grid. This strategic placement is critical for reducing the negative impacts of harmonics, preserving the sinusoidal pattern of the grid's current, and enhancing PQ. The SAPF operates by continually tracking any deformation in the current and extracting the harmonic components using P-Q theory. Once the harmonics have been detected, the SAPF provides a compensatory current of identical amplitude but opposite phase to the harmonic component current. The compensatory current is injected into the grid at the PCC, consequently canceling out the harmonics.

#### *3.3.1 Conventional PQ-Theory for SAPF Control*

The SAPF is controlled by P-Q theory, which employs the PI controller for $V_{dc}$ voltage regulation. Maintaining a steady capacitor terminal voltage is extremely vital process for managing the SAPF. THD was successfully suppressed to 5.25 pointing to the SAPF's effectiveness in suppressing harmonics

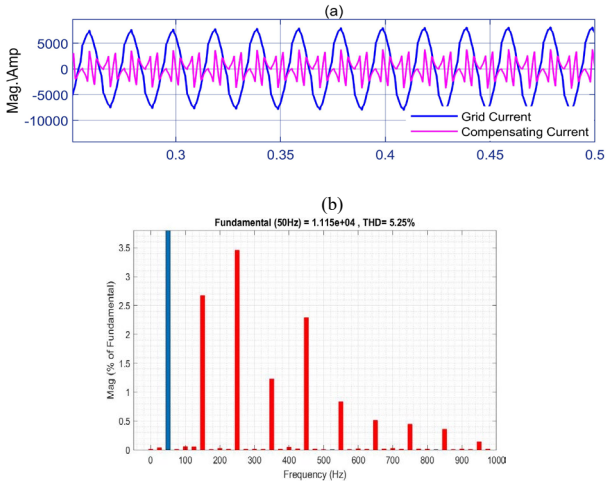


Figure 14. (a) Grid Current (b) Grid Current THD

The SAPF's capacity to inject a compensating current to counteract the harmonic components in the grid current is noticeable, demonstrating the ability of PQ-theory to reduce harmonic distortion.

Although this THD level is lower than the THD recorded after introducing the PV system, it exceeds the limitations specified by IEEE standards, demonstrating the control technique's inability to totally minimize harmonic distortions. The appearance of slightly high THD values highlights the ongoing issue of harmonic elimination in PV-GCS, especially in poor grid circumstances.

The findings indicate the need for more advanced control strategies and optimization techniques to successfully reduce harmonic distortions and increase PQ while adhering to IEEE limitations. Improving these outcomes necessitates additional optimization and the development of novel methodologies. The flowing is an optimization algorithm, directed toward improving control strategies and maximizing the performance of SAPF. These developments will support the smooth integration of solar PV system into the grid, ensuring both stability and efficiency. Maximizing the performance of the SAPF using advanced algorithms requires an accurate definition of an objective function.

#### *3.3.2 GA for SAPF Optimization*

To ensure that the SAPF performs properly, the PI controller parameters must be determined adequately. The objective function is to reduce the error in DC bus capacitor terminal voltage, which is the difference between the real $V_{dc}$ and the desired reference $V_{dc.ref}$ ( $V_{dc} - V_{dc.ref}$), thereby maintain the stability and performance of the SAPF. An optimization algorithm, such as the GA, employed to properly estimate the PI parameters. The

algorithm optimizes parameters to ensure the PI controller can regulate the $V_{dc}$, which is crucial for the SAPF to function smoothly. Figure 15(a) are the filter grid current and harmonic compensating current. Where Figure 15 (b) shows the reduced THD by GA of 4.79. Although this is an improvement over the baseline scenario, additional refinement is required to meet the standards, particularly with $V_{dc}$ voltage regulation.

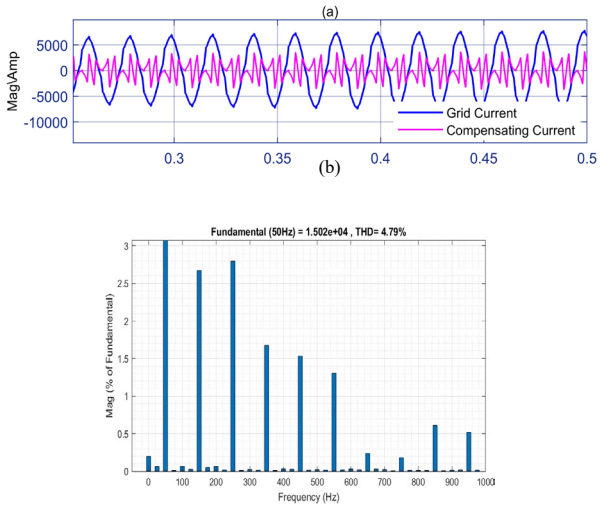


Figure 15. (a) Grid Current (b) Grid Current THD

The GA-based optimization technique holds potential for improving THD in PV-GCS. GA's performance extends beyond harmonic mitigation by analyzing system stability under changing PV conditions

### *3.3.3 PSO for SAPF Optimization*

Introducing PSO to tune the PI controller for the SAPF resulted in considerable harmonic elimination. The PSO algorithm effectively fine-tunes controller parameters, leading to better harmonic mitigation performance.

The results clearly show the effectiveness of PSO in modifying SAPF settings. This is demonstrated in Figure 16 (a), which depicts the grid current and the accompanying harmonic compensating current. The optimized SAPF successfully injects compensating currents to counteract harmonic elements. The grid current is slightly distorted at some levels. The observed THD of 3.72 percent, displayed in Figure 16(b), represents a significant improvement of THD over the earlier control strategy.

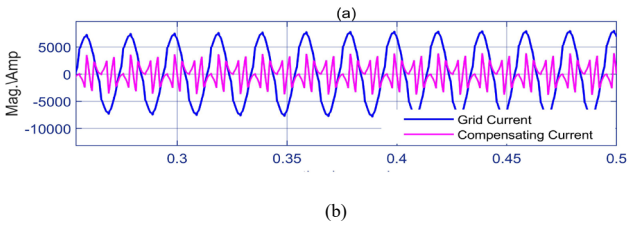


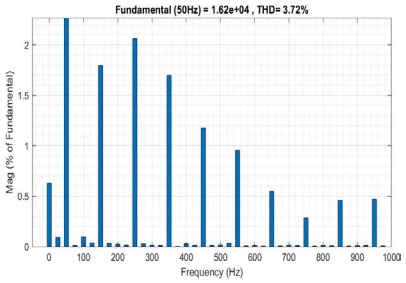


Figure 16. (a) Grid Current (b) Grid Current THD

This improvement highlights the significance of applying advanced optimization techniques to further enhance the operational effectiveness of SAPFs in real-world power systems.

### *3.3.4 GE for SAPF Optimization*

Tuning the SAPF controller with the GE algorithm improved THD. Figure 17 (a) displays the grid current and the harmonic compensating current. The GE algorithm reduced THD to acceptable levels while displaying a grid current with low distortion.

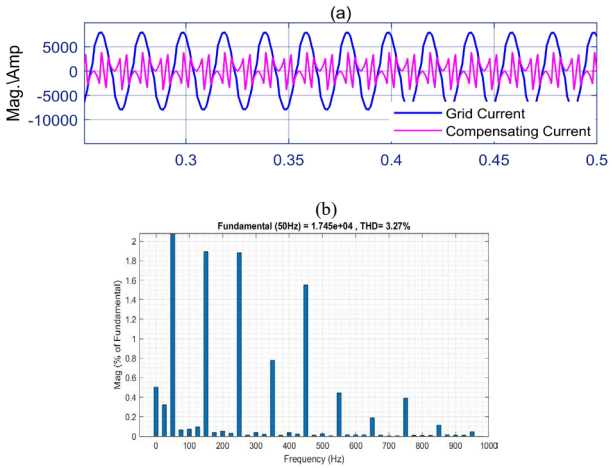


Fig. 17. (a) Grid Current (b) Grid Current THD

The THD level is 3.27 as in Figure 17 (b) is a substantial improvement over previous techniques, illustrating the GE algorithm's ability to reduce harmonic distortion. These outcomes emphasize the capability of GE algorithm in adjusting the parameters dynamically, taking into account load variation and PV output fluctuation.

### *3.3.5 JSO for SAPF Optimization*

Further analysis after leveraging the JSO algorithm reveals significant improvements in THD. The filtered grid current and harmonic compensating current, are shown in Figure 18 (a).

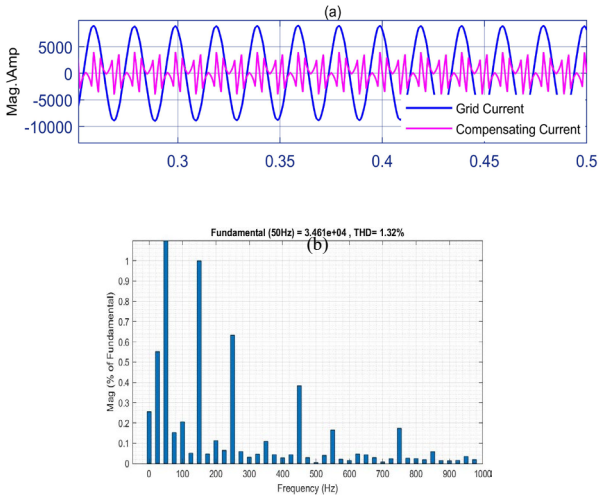


Figure 18. (a) Grid Current (b) Grid Current THD

The grid current is a clean sine wave without noticeable distortion, THD of only 1.32 *percent* as in Figure 18(b). Fine-tuning the PI controller gains using the JSO algorithm leads to faster response times and improved transient performance. As a result, the JSO algorithm finds an effective balance between THD reduction and overall system performance, thus improving overall efficiency. Comparatively, the management of the $V_{dc}$voltage in the SAPF has a profound impact on its performance, particularly harmonic reduction.

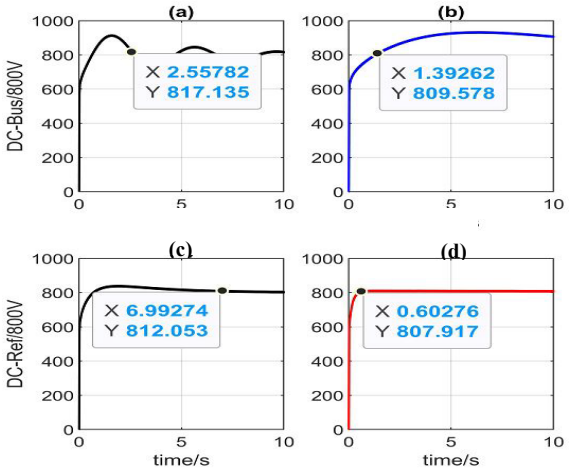


Figure 19. $V_{dc}$ Regulation Curves of Different Algorithms

Figure 19 depicts the $V_{dc}$ voltage regulation curves of different algorithms, demonstrating their different performance characteristics.

The conventional GA has inadequate $V_{dc}$ regulation as in figure 19(a), resulting in excessive grid current THD levels. PSO detects out-of-range voltage, as in graph 19(b), reducing grid current quality. While GE in figure 19(c) adequately maintained steady $V_{dc}$ with long settling time. JSO algorithm in curve 19(d) demonstrate superiority in reducing harmonics in PV-GCS is supported by its improved $V_{dc}$ voltage control and significant reduction in THD. These results show the JSO algorithm's capabilities to preserve system stability and increase power PQ, making it a proper solution for increasing SAPF performance in real-world applications.

Table 2. Algorithm's Performance Comparison

| Algorithm | Algorithm Characteristics | | | THD % | Parameter | |
|---|---|---|---|---|---|---|
| | Spead response | conver -gence | Enhance $V_{dc}$ | | $k_p$ | $k_i$ |
| GA | moderate | low | poor | 4.79 | 50 | 400 |
| PSO | slow | effec | poor | 3.72 | 500 | 200 |
| GE | fast | high | moderate | 3.27 | 50 | 100 |
| JSO | Fast | high | effective | 1.32 | 600 | 450 |

Table 2 highlights the compression of four algorithms in terms of speed response, convergence, and voltage regulation. The outcome gives insight into the performance of each algorithm in harmonic mitigation.

## 4. CONCLUSION

This work presents novel methods for harmonic mitigation in PV-GCS using sophisticated metaheuristic optimization approaches, with an emphasis on the JSO algorithm for the SAPF. The JSO algorithm outperforms other methods by providing adaptive and robust solutions for real-time harmonic reduction. The simulation results indicate a considerable reduction in THD from 14.10% to 1.32%, indicating the JSO algorithm's better harmonic mitigation capabilities and improving. Additionally, the $V_{dc}$ voltage was efficiently regulated, with the value settling at 807V in 0.6 seconds, demonstrating the system's rapid response. The study thoroughly studied the issues posed by NLL in LV feeder and the intermittent nature of PV generation. The JSO method proved to be the most effective optimization strategy, offering significant increases in harmonic reduction while keeping $V_{dc}$ regulation within acceptable bounds with a rapid settling time. The combination of instantaneous reactive power theory with metaheuristic optimization algorithms, notably the JSO, shows a 90.6% improvement in THD reduction compared to traditional techniques. These findings highlight the JSO algorithm's potential for addressing the expanding complexities of modern power systems, particularly those that include solar PV. JSO's successful application in both harmonic distortion reduction and voltage control demonstrates its effectiveness and future applicability in renewable energy systems.

## ACKNOWLEDGMENT

The research work was supported by State Grid Science & Technology Project "Research on Key Technologies for Energy Sharing Market Operation with Multiple Flexible

Resource Participation". (5400-202316589A-3-2-ZN), Hubei Engineering and Technology Research Center for AC/DC Intelligent Distribution Network, School of Electrical Engineering and Automation, Wuhan, University.Wuhan 430072.

## REFERENCES

[1] Energy Development, Challenges, and Policies of Leading Indian States with an International Perspective," 2020, *Institute of Electrical and Electronics Engineers Inc.* doi: 10.1109/ACCESS.2020.2988011.

[2] Q. Hassan, M. Al-Hitmi, V. S. Tabar, A. Z. Sameen, H. M. Salman, and M. Jaszczur, "Middle East energy consumption and potential renewable sources: An overview," *Clean Eng Technol*, vol. 12, Feb. 2023, doi: 10.1016/j.clet.2023.100599.

[3] E. Zhao, Y. Han, X. Lin, E. Liu, P. Yang, and A. S. Zalhaf, "Harmonic characteristics and control strategies of grid-connected photovoltaic inverters under weak grid conditions," *International Journal of Electrical Power and Energy Systems*, vol. 142, Nov. 2022, doi: 10.1016/j.ijepes.2022.108280.

[4] A. N. Abdalla *et al.*, "Integration of energy storage system and renewable energy sources based on artificial intelligence: An overview," *J Energy Storage*, vol. 40, Aug. 2021, doi: 10.1016/j.est.2021.102811.

[5] S. Dey, A. Sreenivasulu, G. T. N. Veerendra, K. V. Rao, and P. S. S. A. Babu, "Renewable energy present status and future potentials in India: An overview," Sep. 01, 2022, *Elsevier B.V.* doi: 10.1016/j.igd.2022.100006.

[6] V. A. Sulibhavi and S. G. Ankaliki, "Harmonic Analysis of Non-Linear Loads in Distribution System and Mitigation Using Passive Filters," *International Research Journal of Engineering and Technology*, 2022, [Online]. Available: www.irjet.net

[7] S. Janpong, K. Areerak, and K. Areerak, "Harmonic detection for shunt active power filter using adaline neural network," *Energies (Basel)*, vol. 14, no. 14, Jul. 2021, doi: 10.3390/en14144351.

[8] S. Rustemli, M. A. Satici, G. Şahin, and W. van Sark, "Investigation of harmonics analysis power system due to non-linear loads on the electrical energy quality results," *Energy Reports*, vol. 10, pp. 4704–4732, Nov. 2023, doi: 10.1016/j.egyr.2023.11.034.

[9] T. Belgore Lecturer and G. Najashi HOD, "Control Techniques for Shunt Active Power Filters." [Online]. Available: www.ijert.org

[10] S. M. Ahsan, H. A. Khan, A. Hussain, S. Tariq, and N. A. Zaffar, "Harmonic analysis of grid-connected solar PV systems with nonlinear household loads in low-voltage distribution networks," *Sustainability (Switzerland)*, vol. 13, no. 7, Apr. 2021, doi: 10.3390/su13073709.

[11] R. Kumar, "Fuzzy particle swarm optimization control algorithm implementation in photovoltaic integrated shunt active power filter for power quality improvement using hardware-in-the-loop," *Sustainable Energy Technologies and Assessments*, vol. 50, Mar. 2022, doi: 10.1016/j.seta.2021.101820.

[12] T. Gayibov, S. Latipov, D. Abdurashidov, B. Pulatov, and A. Davirov, "Algorithm for power systems mode optimization taking into account the frequency change in terms of probablistic nature of initial information," in *IOP Conference Series: Materials Science and Engineering*, IOP Publishing Ltd, Jul. 2020. doi: 10.1088/1757-899X/883/1/012185.

[13] B. Amini, H. Rastegar, and M. Pichan, "An optimized proportional resonant current controller based genetic algorithm for enhancing shunt active power filter performance," *International Journal of Electrical Power and Energy Systems*, vol. 156, Feb. 2024, doi: 10.1016/j.ijepes.2023.109738.

[14] B. Sahoo, M. M. Alhaider, and P. K. Rout, "Power quality and stability improvement of microgrid through shunt active filter control application: An overview," *Renewable Energy Focus* , vol. 44, pp. 139–173, Mar. 2023, doi: 10.1016/j.ref.2022.12.006.

[15] S. B. Mohanty and S. Mohanty, "Modified Asymmetrical H-Bridge MLI With Minimum Switching Loss and Harmonic Distortion Using JAYA Algorithm," *IEEE Access*, vol. 12, pp. 78854–78864, 2024, doi: 10.1109/ACCESS.2024.3406781.

[16] M. L. Duc, L. Hlavaty, P. Bilik, and R. Martinek, "Harmonic Mitigation Using Meta-Heuristic Optimization for Shunt Adaptive Power Filters: A Review," May 01, 2023, *MDPI*. doi: 10.3390/en16103998.

[17] R. Kanagavel and V. Indragandhi, "Current control techniques of single phase shunt active power filter-a review," in *IOP Conference Series: Materials Science and Engineering*, Institute of Physics Publishing, Oct. 2019. doi: 10.1088/1757-899X/623/1/012007.

[18] A. Alam *et al.*, "Jellyfish search optimization algorithm for mpp tracking of pv system," *Sustainability (Switzerland)*, vol. 13, no. 21, Nov. 2021, doi: 10.3390/su132111736.

[19] J. S. Chou and A. Molla, "Recent advances in use of bio-inspired jellyfish search algorithm for solving optimization problems," *Sci Rep*, vol. 12, no. 1, Dec. 2022, doi: 10.1038/s41598-022-23121-z.

[20] A. M. Nassef, M. A. Abdelkareem, H. M. Maghrabie, and A. Baroutaji, "Review of Metaheuristic Optimization Algorithms for Power Systems Problems," Jun. 01, 2023, *Multidisciplinary Digital Publishing Institute (MDPI)*. doi: 10.3390/su15129434.

[21] M. Merai, M. W. Naouar, I. Slama-Belkhodja, and E. Monmasson, "An Adaptive PI Controller Design for DC-Link Voltage Control of Single-Phase Grid-Connected Converters," *IEEE Transactions on Industrial Electronics*, vol. 66, no. 8, pp. 6241–6249, Aug. 2019, doi: 10.1109/TIE.2018.2871796.

[22] Y. Hoon, M. A. M. Radzi, M. A. A. M. Zainuri, and M. A. M. Zawawi, "Shunt active power filter: A review on phase synchronization control techniques," Jul. 01, 2019, *MDPI AG*. doi: 10.3390/electronics8070791.

[23] A. Kalair, N. Abas, A. R. Kalair, Z. Saleem, and N. Khan, "Review of harmonic analysis, modeling and mitigation techniques," 2017, *Elsevier Ltd*. doi: 10.1016/j.rser.2017.04.121.

[24] T. O. Araoye, E. C. Ashigwuike, A. C. Adeyemi, S. V. Egoigwe, N. G. Ajah, and E. Eronu, "Reduction and control of harmonic on three-phase squirrel cage induction motors with voltage source inverter (VSI) using ANN-grasshopper optimization shunt active filters (ANN-GOSAF)," *Sci Afr*, vol. 21, Sep. 2023, doi: 10.1016/j.sciaf.2023.e01785.

[25] A. Shah and N. Vaghela, "Shunt Active Power Filter for Power Quality Improvement in Distribution Systems | Shunt Active Power Filter for Power Quality Improvement in Distribution Systems", [Online]. Available: www.ijedr.org

[26] A. A. Imam, R. Sreerama Kumar, and Y. A. Al-Turki, "Modeling and simulation of a pi controlled shunt active power filter for power quality enhancement based on p-q theory," *Electronics (Switzerland)*, vol. 9, no. 4, Apr. 2020, doi: 10.3390/electronics9040637.

[27] S. Kumaresan and H. Habeebullah Sait, "Design and control of shunt active power filter for power quality improvement of utility powered brushless DC motor drives," *Automatika*, vol. 61, no. 3, pp. 507–521, Jul. 2020, doi: 10.1080/00051144.2020.1789402.

[28] S. Khalid, "A novel Algorithm Adaptive Autarchoglossans Lizard Foraging (AALF) in a shunt active power filter connected to MPPT-based photovoltaic array," *e-Prime - Advances in Electrical Engineering, Electronics and Energy*, vol. 3, Mar. 2023, doi: 10.1016/j.prime.2022.100100.

[29] M. F. Roslan, A. Q. Al-Shetwi, M. A. Hannan, P. J. Ker, and A. W. M. Zuhdi, "Particle swarm optimization algorithm-based PI inverter controller for a grid-connected PV system," *PLoS One*, vol. 15, no. 12 December, Dec. 2020, doi: 10.1371/journal.pone.0243581.

[30] A. Mohammadi-Balani, M. Dehghan Nayeri, A. Azar, and M. Taghizadeh-Yazdi, "Golden eagle optimizer: A nature-inspired metaheuristic algorithm," *Comput Ind Eng*, vol. 152, Feb. 2021, doi: 10.1016/j.cie.2020.107050.

[31] J. S. Chou and D. N. Truong, "A novel metaheuristic optimizer inspired by behavior of jellyfish in ocean," *Appl Math Comput*, vol. 389, Jan. 2021, doi: 10.1016/j.amc.2020.125535.

[32] H. A. I. Gony, G. I. Rashed, A. Badjan, O. M. Ahmed Bahageel, H. Hualiang, and H. I. Shaheen, "Bat Algorithm-Based Shunt Active Power Filter for Harmonics Control in PV Grid-Connected Systems under Nonlinear Load," in *Proceedings - 2024 9th Asia Conference on Power and Electrical Engineering, ACPEE 2024*, Institute of Electrical and Electronics Engineers Inc., 2024, pp. 635–639. doi: 10.1109/ACPEE60788.2024.10532587.